Dually pH/Reduction-Responsive Vesicles for Ultrahigh-Contrast Fluorescence Imaging and Thermo-Chemotherapy-Synergized Tumor Ablation

Aijun Zhu,[†,∥] Ke Miao,[‡,∥] Yibin Deng,[†] Hengte Ke,[†] Hui He,[†] Tao Yang,[†] Miao Guo,[†] Yanli Li,[†] Zhengqing Guo,[§] Yangyun Wang,[§] Xiangliang Yang,[⊥] Youliang Zhao,[*,‡] and Huabing Chen[*,†,§]

[†]Jiangsu Key Laboratory of Translational Research and Therapy for Neuro-Psycho-Diseases, and College of Pharmaceutical Sciences, Soochow University, Suzhou, Jiangsu 215123, China, [‡]Jiangsu Key Laboratory of Advanced Functional Polymer Design and Application, and College of Chemistry, Chemical Engineering and Materials Science, Soochow University, Suzhou , Jiangsu 215123, China, [§]School of Radiological and Interdisciplinary Sciences (RAD-X), Collaborative Innovation Center of Radiation Medicine of Jiangsu Higher Education Institutions, and School of Radiation Medicine and Protection, Soochow University, Suzhou, Jiangsu 215123, China, and [⊥]College of Life Science and Technology, Huazhong University of Science and Technology, Wuhan 430074, China. [∥]These authors contributed equally.

ABSTRACT Smart nanocarriers are of particular interest as nanoscale vehicles of imaging and therapeutic agents in the field of theranostics. Herein, we report dually pH/reduction-responsive terpolymeric vesicles with monodispersive size distribution, which are constructed by assembling acetal- and disulfide-functionalized star terpolymer with near-infrared cyanine dye and anticancer drug. The vesicular nanostructure exhibits multiple theranostic features including on-demand drug releases responding to pH/reduction stimuli, enhanced photothermal conversion efficiency of cyanine dye, and efficient drug translocation from lysosomes to cytoplasma, as well as preferable cellular uptakes and biodistribution. These multiple theranostic features result in ultrahigh-contrast fluorescence imaging and thermo-chemotherapy-synergized tumor ablation. The dually stimuli-responsive vesicles represent a versatile theranostic approach for enhanced cancer imaging and therapy.

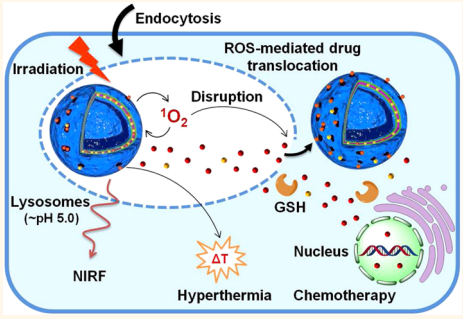

KEYWORDS: vesicles · stimuli-responsive release · cancer imaging · photothermal therapy · synergistic effect

Nanocarriers have been considered as emerging theranostic vehicles in the field of cancer detection and therapy.[1−4] Various nanocarriers are designed to achieve fluorescence, ultrasonics, magnetic resonance imaging, and positron emission tomography for precise tumor detection,[5,6] and simultaneously hold great potentials as drug vehicles for cancer-targeted therapy.[3,4,7,8] In particular, smart nanocarriers are able to trigger signal activation or smart drug release in response to tumor microenvironments.[9−14] For instance, stimuli-responsive chemistry was reported to improve signal-to-noise ratio of fluorescent dyes or drug accumulation in cancer cells for enhanced imaging contrast or anticancer efficacy.[9−19] To date, despite recent progress in the exploration of smart nanocarriers for cell imaging with high contrast,[18−21] there are still only a few applicable smart nanocarriers to achieve *in vivo* imaging with high contrast owing to limited signal retention at tumor and undesired noise at normal tissues.[12,22,23] Moreover, it is difficult to provide effective stimuli-responsive drug delivery upon further incorporation of anticancer compounds within same nanocarriers, since anticancer compounds often have different intracellular trafficking to target sites as compared to imaging agents.[5,10,11,24] The exploration of smart theranostic nanoparticles encounters multiple limitations such as difficult preparation, insufficient drug loading, limited targeting ability, as well as

* Address correspondence to ylzhao@suda.edu.cn; chenhb@suda.edu.cn.

Received for review September 30, 2014 and accepted July 16, 2015.

Published online July 16, 2015
10.1021/acsnano.5b02843

© 2015 American Chemical Society

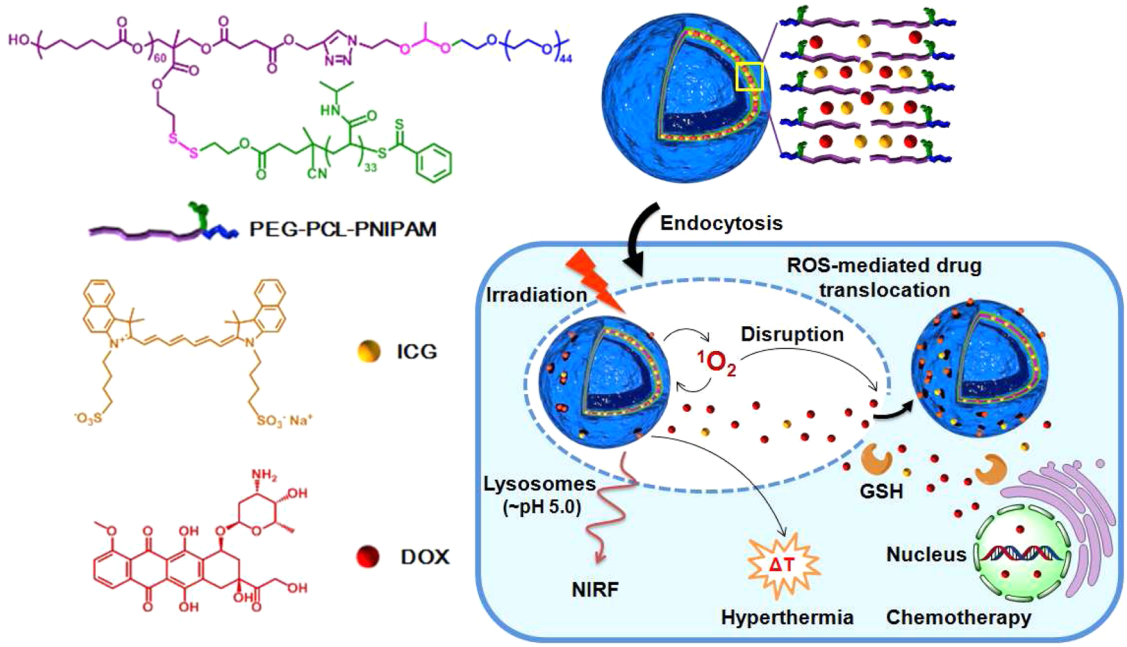

Scheme 1. Illustration of dually pH/reduction-responsive terpolymeric Vesicles for NIRF imaging with ultrahigh contrast and synergistic anticancer efficacy.

unsatisfactory imaging or therapeutic responsiveness. Consequently, it is a major challenge to develop a new smart nanocarrier with desired theranostic features for both cancer imaging with ultrahigh contrast and optimal anticancer efficacy.[1,2,5]

Recently, near-infrared cyanine dyes such as indocyanine green (ICG) have been developed as theranostic agents, which possess bifunctional properties including near-infrared fluorescence (NIRF) and photothermal effect under light irradiation for theranostic application.[25,26] The nanocarriers including micelles, polymeric nanoparticles, and liposomes can effectively deliver these bifunctional cyanine dyes for both NIRF imaging and photothermal therapy (PTT).[27−33] Moreover, the nanocarriers such as micelles are found to achieve synergistic thermo-chemotherapy or thermo-photodynamic therapy owing to their sustained releases, preferable tumor accumulation, and enhanced drug translocation from lysosomes to cytoplasm upon coencapsulation with anticancer compounds such as doxorubicin and chlorin e6.[27,30] However, the design of the existing theranostic nanocarriers such as micelles is mainly limited in several aspects: first, detectable NIRF signals at tumors are generally diminished quickly owing to easy degradation and elimination of cyanine dyes in physiological environment (*e.g.*, lysosomes) upon release from nanocarriers, and thus cause unsatisfied imaging contrast for cancer imaging; second, so far there is a lack of effective strategy to regulate photothermal conversion efficiency of cyanine dye for generating stronger hyperthermia ability to improve PTT efficacy; third, for the application in thermo-chemotherapy, cyanine dyes often require low intracellular release from nanocarrier for overcoming their poor chemical stability and yet anticancer drugs often demand enhanced release in cancer cells, while the existing nanocarriers such as micelles are unable to satisfy their various intracellular release demands. Thus, the nanocarriers are required to coordinate their various release behaviors, and regulate the photothermal effect of cyanine dye for achieving respective functions. Hence, it is highly necessary to explore a smart nanocarrier for both ultrahigh-contrast cancer NIRF imaging and preferably synergistic thermo-chemotherapy.

Polymeric vesicles are being developed as an effective nanocarrier for cancer therapy, which are often self-assembled from synthetic amphiphilic copolymers or polyion complex.[34] Therapeutic compounds can be encapsulated into hydrophilic chamber or hydrophobic membranes in polymeric vesicles, which are reported to possess diverse properties such as good stability, enhanced cellular uptake, long circulation and preferable biodistribution.[35,36] Recently, several stimuli-responsive vesicles have been developed to improve the intracellular release of anticancer compounds responding to pH, temperature, and enzymes.[37] To date, there are a few reports on smart polymeric vesicles for *in vivo* theranostic application. For instance, it is still difficult to design polymeric vesicles for regulating both imaging and therapeutic agents for desired theranostic properties. As a proof-of-concept, we report dually pH/reduction-responsive terpolymeric vesicles with multiple theranostic features for both ultrahigh-contrast NIRF imaging and preferably synergistic thermo-chemotherapy with tumor ablation (Scheme 1). The vesicles encapsulating cyanine dye (indocyanine

green, ICG) and anticancer drug (doxorubicin, DOX) can coordinate their respective on-demand releases, and simultaneously improve the photothermal conversion efficiency of ICG. Thus, the vesicles induce NIRF imaging of ICG with ultrahigh contrast owing to its reduced release responding to pH stimulus and subsequent fluorescence dequenching, as well as enhanced tumor accumulation and retention. Simultaneously, the vesicular structures exhibit the enhanced photothermal effect of ICG, and also induce highly efficient translocation of DOX from lysosomes to cytoplasma *via* its pH/reduction-responsive release and reactive oxygen species (ROS)-mediated lysosomal disruption, which synergistically results in effective thermo-chemotherapy with tumor ablation. The pH/reduction-responsive vesicular nanostructures provide a valuable approach to constitute smart theranostic nanoplatform with desirable properties.

RESULTS AND DISCUSSION

Synthesis, Preparation, and Characterization. To achieve this goal, a pH/reduction-cleavable star terpolymer, poly(ethylene glycol)−poly(ε-caprolactone)−poly(*N*-isopropylacrylamide) (PEG−PCL−PNIPAM), was synthesized through multiple procedures as shown in Figure 1A, and the detailed methods were described in Supporting Information. First, a multifunctional agent 2-((2-((2-hydroxymethyl-2-((4-oxo-4-(prop-2-yn-1-yloxy)butanoyl)oxy)-methyl)propionyloxy)ethyl)disulfanyl)ethyl 4-cyano-4-(phenylcarbonothioylthio)pentanoate (HCP) was used to initiate ring-opening polymerization (ROP) of ε-caprolactone (CL) to afford PCL. Second, PCL-*b*-PNIPAM was synthesized by reversible addition−fragmentation chain transfer (RAFT) polymerization of *N*-isopropylacrylamide (NIPAM) mediated by PCL macro chain transfer agent.[38,39] Last, acetal- and disulfide-functionalized PEG_{45}−PCL_{60}−$PNIPAM_{33}$ ($M_{n,NMR}$ = 13200 g/mol, and $M_{n,GPC}$ = 20 700 g/mol) with narrow molecular weight distribution (PDI = 1.14) was obtained by Cu(I)-mediated azide−alkyne cycloaddition reaction between PEG-*acetal*-N_3 and alkyne-functionalized PCL-*b*-PNIPAM (Supporting Information Table S1).[40] ^{1}H NMR spectra, GPC, and GPC-MALLS fully confirmed the chemical structures and compositions of the star terpolymer and its precursors (Figure 1B and Supporting Information Figures S1−S8).

Subsequently, the cleavage of PEG_{45}−PCL_{60}−$PNIPAM_{33}$ responding to pH and reduction stimuli was evaluated using GPC analysis. When the polymer was exposed to pH 5.0 and 10 mM dithiothreitol (DTT) at 37 °C for 48 h, the detached PCL−PNIPAM ($M_{n,GPC}$ = 17 100 g/mol) and PEG−PCL ($M_{n,GPC}$ = 15 300 g/mol) were generated, respectively (Supporting Information Figure S9). It indicates that the apparent molecular weight of detached PCL−PNIPAM was close to that of its original diblock copolymer (PCL−PNIPAM, $M_{n,GPC}$ = 17 600 g/mol) as shown in Supporting Information

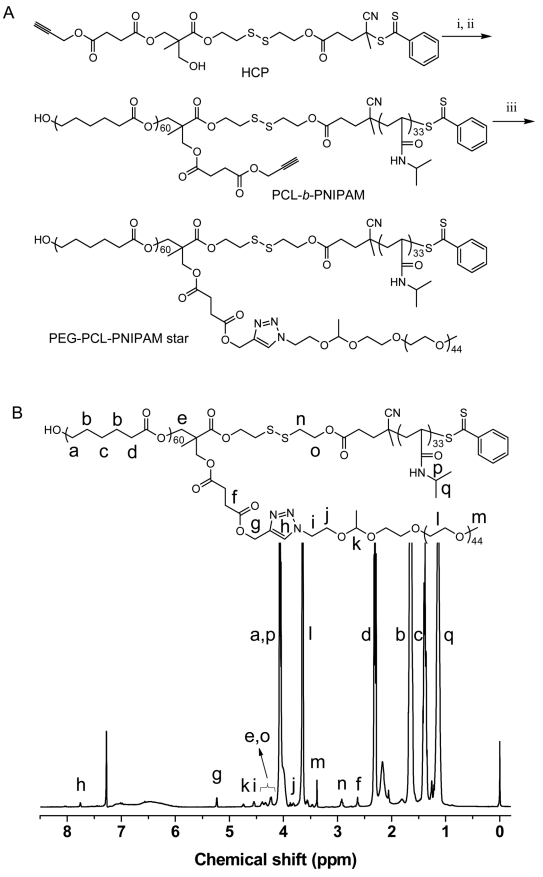

Figure 1. (A) Synthesis of acetal and disulfide functionalized PEG−PCL−PNIPAM star terpolymer: (i) CL, ROP; (ii) NIPAM, RAFT; (iii) PEG*acetal*-N_3, CuBr, PMDETA. (B) ^{1}H NMR spectrum of PEG_{45}-PCL_{60}-$PNIPAM_{33}$.

Figure S5. Obviously, the star terpolymer can be cleaved in response to pH/reduction stimuli.

PEG_{45}−PCL_{60}−$PNIPAM_{33}$ (6.0 mg), ICG (2.0 mg) and DOX (2.0 mg) were dissolved in the mixture of methanol and triethylamine, which was evaporated into the uniform membranes, followed by the dispersion into water, purification, and subsequent formation of ICG/DOX-loaded PEG_{45}−PCL_{60}−$PNIPAM_{33}$ vesicles (Vesicles). Transmission electron microscopy (TEM) imaging shows that Vesicles possess the uniform vesicular morphology with average size of 101.2 ± 10.5 nm (Figure 2A). Vesicles had an average hydrodynamic diameter of 158.2 nm with particle size distribution of 0.102 measured by dynamic light scattering (Figure 2B). Obviously, Vesicles possess a monodispersive vesicular nanostructure in aqueous solution.[29] Next, the entrapment efficiencies of ICG and DOX within Vesicles were evaluated using ultrafilter centrifuge with 100 kDa membrane filters. ICG (99.0%) and DOX (80.0%) were entrapped within Vesicles at the total drug loading level of 40% each, possibly owing to the good encapsulation of ICG and DOX within vesicular membranes.

The stability of encapsulated agents is a prerequisite for cancer theranostics, and thus, we evaluated the chemical stability of ICG and DOX in Vesicles in the

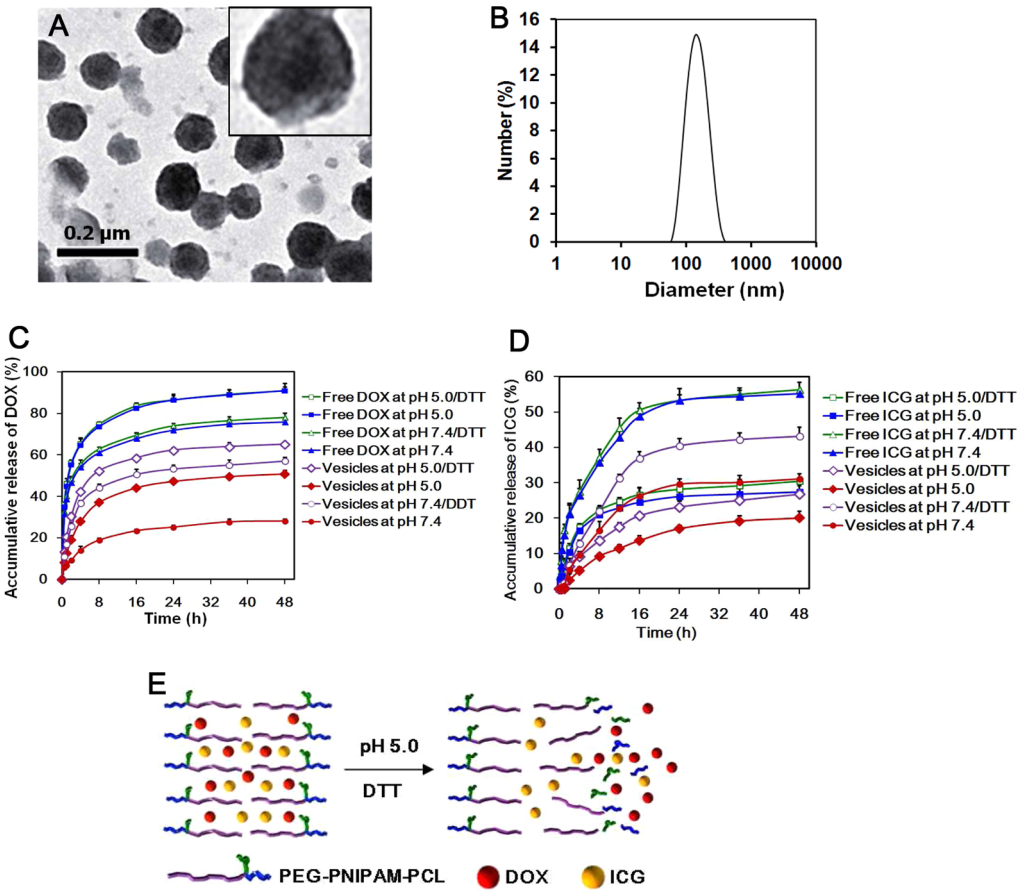

Figure 2. (A) TEM image of Vesicles. (B) Size distribution of Vesicles measured using dynamic light scattering. (C) Normalized releases of DOX from Vesicles and free ICG/DOX in various solutions. (D) Normalized releases of ICG from Vesicles and free ICG/DOX in various solutions. (E) Release illustration of ICG and DOX from Vesicles responding to pH/reduction stimuli.

various solutions at 25 °C. Supporting Information Figure S10 shows that Vesicles exhibited good stability of ICG and DOX in the various solutions including serum, cell culture medium, and buffers pH 7.4 and pH 5.0 during 48 h as compared to free ICG and DOX.[30] The good stability might be attributed to the good encapsulation of ICG and DOX within the vesicles, indicating that Vesicles are capable to protect ICG and DOX from the degradation in physiological or acidic environment.

On-Demand Drug Releases. Drug release plays an important role for intracellular delivery of anticancer drug, but may impair imaging contrast and PTT efficacy of ICG owing to its poor stability upon exposure in aqueous environment. Then, we demonstrated the release behaviors of DOX and ICG from Vesicles at various pH and reduction stimuli at 37 °C. Vesicles exhibited the sustained releases of both DOX and ICG in PBS at pH 7.4 as compared to the mixture of free ICG and DOX (free ICG/DOX) (Figure 2C,D), indicating that Vesicles are able to minimize their undesirable releases. Importantly, Vesicles exhibited an enhanced release of DOX at pH 5.0 or 10 mM DTT, and the presence of both pH 5.0 and DTT further improved the release of DOX from Vesicles (Figure 2C).[11,17,41] We further synthesized PEG_{45}-*b*-PCL_{66} for constructing ICG/DOX-loaded PEG_{45}-*b*-PCL_{66} micelles (Micelles, 75.7 ± 10.5 nm) as the control without stimulus-responsiveness, which exhibited no responsive release of DOX as compared to Vesicles (Supporting Information Figure S11).[30] The enhanced release of DOX from Micelles just attributed to the protonation of DOX itself at low pH. Remarkably, Vesicles can provide preferable release of DOX responding to pH/reduction stimuli in accordance with the cleavable behavior of star terpolymer (Figure 2E), which might trigger the gradual dissociation of Vesicles, and thus facilitate intracellular release of DOX. On the other hand, we observed that Vesicles had the decreased release of ICG at pH 5.0 or pH 5.0/DTT as compared to that at pH 7.4 (Figure 2D), which is highly potential to improve the chemical stability of ICG for enhanced NIRF imaging and PTT (Supporting Information Figure S10), since released ICG might suffer from degradation in aqueous solution. Possibly, the reduced release of ICG resulted from its protonation, which might induce its hydrophobicity and thus stronger interaction with the polymers in vesicles.[42] Thus, pH/reduction-responsive Vesicles can coordinate the on-demand release behaviors of imaging agent and anticancer drug.

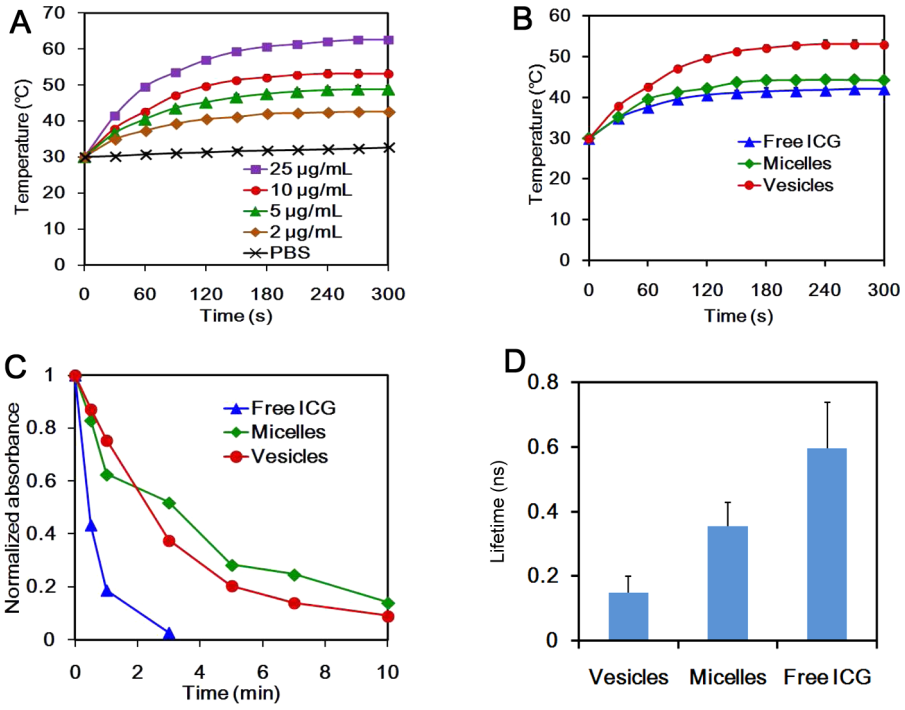

Figure 3. (A) Photothermal profiles of Vesicles containing various concentrations of ICG under 1.5 W/cm^2 irradiation. (B) Photothermal profiles of Vesicles, Micelles, and free ICG/DOX at the dose of 10.0 μg/mL ICG. (C) Normalized absorbances of ICG from Vesicles, Micelles, and free ICG/DOX at various time under 1.5 W/cm^2 irradiation. (D) Fluorescence lifetime of Vesicles, Micelles, and free ICG containing 10.0 μg/mL ICG in aqueous solutions.

Photothermal Conversion Efficiency and Singlet Oxygen Quantum Yield. To demonstrate the capacity of Vesicles to improve photothermal conversion efficiency, we measured their thermal behaviors in aqueous solutions under irradiation. Vesicles exhibited a quick increase of temperature from 30 to 42 °C in 300 s at the concentration of 2.0 μg/mL ICG upon irradiation (Figure 3A),[30] while PBS as a control did not trigger the increase of temperature. Obviously, Vesicles can quickly generate hyperthermia even at a low concentration of ICG, and also exhibited the concentration-dependent thermal increase, which plays an important role to cause cell damage (above 42 °C). Moreover, Figure 3B shows that Vesicles (10.0 μg/mL ICG) triggered a remarkable temperature increase (ΔT = 23.2 °C), which is much higher than those of free ICG/DOX (ΔT = 12.1 °C) and Micelles (ΔT = 14.3 °C). Obviously, the vesicular nanostructures exhibit stronger ability to improve photothermal conversion efficiency of ICG over free ICG/DOX and Micelles.[30] Even though the photostability might account for the slight difference of temperature increase among free ICG/DOX, Micelles, and Vesicles (Figure 3C), it is not the key reason for the enhanced thermal effect of Vesicles.[30] To elucidate the photothermal capacity of Vesicles, we further evaluated their fluorescence lifetime (Figure 3D). Vesicles exhibited the calculated lifetime of 0.15 ns, which is much shorter than that of Micelles (0.35 ns) and free ICG (0.60 ns). Obviously, Vesicles have the enhanced nonradiative transition of ICG within spatially confined vesicular membranes, which might account for their higher photothermal conversion efficiency. So far, there are only a few strategies to improve photothermal conversion efficiency of organic cyanine dyes.[43] The vesicular nanostructure is considered as a new effective regimen for achieving superior photothermal conversion efficiency of organic dyes.

Subsequently, we further measured the singlet oxygen quantum yield of ICG from Vesicles, Micelles and free ICG. The results show that Vesicles had a singlet oxygen quantum yield (Φ_Δ) of 0.32, which is higher than those of Micelles (Φ_Δ = 0.26) and free ICG (Φ_Δ = 0.21) as shown in Supporting Information Figure S12. It indicates that Vesicles might provide stronger ability to generate singlet oxygen as compared to Micelles and free ICG, implying that Vesicles are highly preferable to the damage on the lysosomal membranes *via* photochemical internalization effect of singlet oxygen.[30]

Cellular Uptakes, Endocytic Pathways, Intracellular Distribution, and Thermo-Chemotherapeutic Cytotoxicity. To demonstrate the capacity of Vesicles to facilitate cellular uptakes of ICG and DOX by cancer cells, we evaluated their internalized amounts by 4T1 cells.[30] Vesicles remarkably improved the cellular uptakes of ICG and DOX after 24 h incubation as compared to free ICG/DOX and Micelles, respectively (Figure 4A). Obviously, Vesicles possess superior capacity to improve the cellular uptakes of encapsulated agents, which are advantageous to generate the concentration-dependent

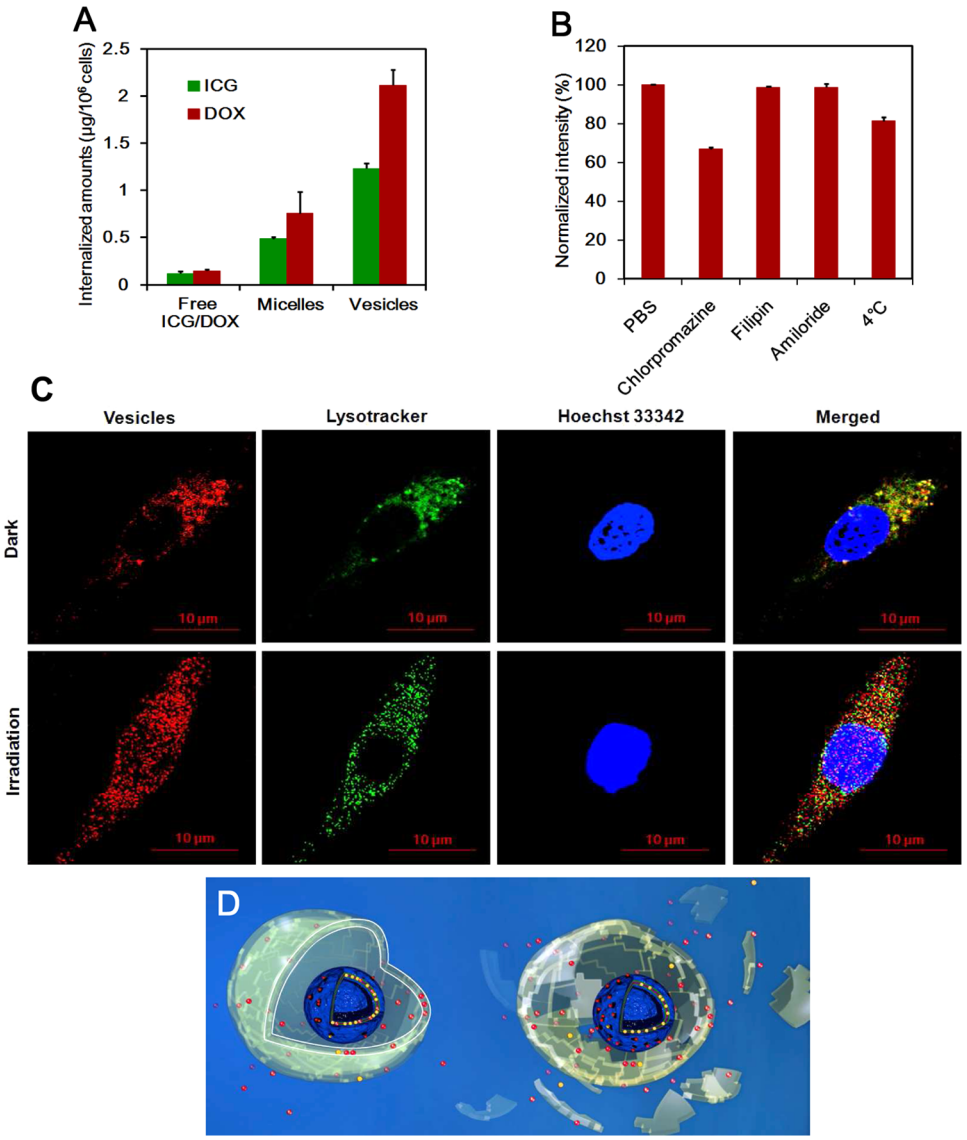

Figure 4. (A) Internalized amounts of ICG from Vesicles, Micelles and free ICG/DOX at the dose of 4.0 μg/mL ICG by 4T1 cells after 24 h incubation. (B) Relative intensities of DOX from Vesicles (4.0 μg/mL DOX) internalized by 4T1 cells treated with PBS (control), chlorpromazine (10.0 mg/mL), filipin (5.0 mg/mL), amiloride (100.0 mg/mL) at 37 °C, and PBS at 4 °C using flow cytometry. (C) CLSM images of 4T1 cells stained by Lysotracker Green DND-26 and Hoechst 33342 after 0.5 h incubation with Vesicles under darkness and irradiation (785 nm, 3 min, 1.5 W/cm^2). (D) Schematic illustration of ROS-mediated lysosomal disruption triggered by Vesicles under irradiation.

hyperthermia in cells and improve the intracellular accumulation of DOX as well. Next, the endocytic pathways of Vesicles were further evaluated using flow cytometry. Chlorpromazine as an inhibitor of clathrin-mediated endocytosis led to the decrease of 38% in the cellular uptake of DOX (Figure 4B), indicating that Vesicles are effectively internalized into endocytic compartments *via* the clathrin-mediated endocytosis.[29]

We further employed confocal laser scanning microscopy (CLSM) to observe the intracellular distribution of Vesicles in 4T1 cells stained by Lysotracker Green DND-26 and Hoechst 33342. Figure 4C shows that Vesicles had the colocalization of 92.5% with the lysosomes, indicating that Vesicles can quickly be distributed into the lysosomes *via* the endocytosis under darkness. Interestingly, Vesicles only exhibited the colocalization level of 9.5% with the lysosomes after irradiation (Figure 4C). Remarkably, Vesicles triggered the translocation of DOX into the cytoplasma and nucleus upon irradiation. To further validate the lysosomal disruption induced by Vesicles under irradiation, acridine orange (AO) staining was used to evaluate the integrity of the lysosomes.[29,30] Supporting Information Figure S13 shows that the cells treated with PBS under the darkness and irradiation displayed overlapped yellow fluorescence between red and green fluorescence, indicating that PBS had no influence on the integrity of the lysosomes under irradiation or not. However, the yellow fluorescence from AO was decreased under irradiation when the concentrations

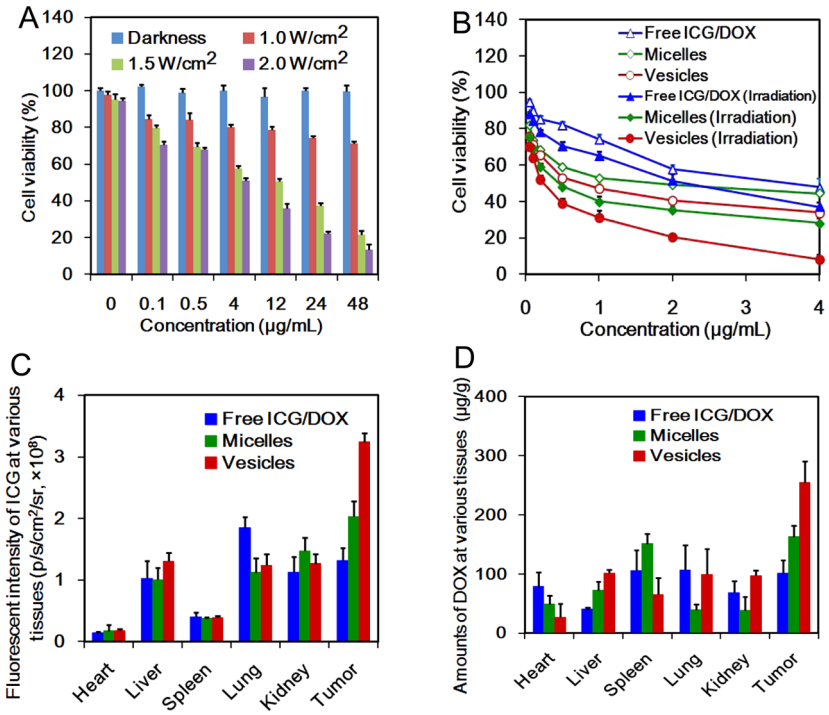

Figure 5. (A) Cell viability of 4T1 cells treated with ICG-Vesicles at various concentrations under darkness, and 1.0, 1.5, and 2.0 W/cm^2 irradiation (785 nm, 3 min), respectively. (B) Cell viability of 4T1 cells treated with Vesicles, Micelles and free ICG/DOX under 1.5 W/cm^2 irradiation (785 nm, 3 min). (C) *Ex vivo* distribution of ICG, and (D) accumulative amounts of DOX from Vesicles, Micelles, and free ICG/DOX in heart, liver, spleen, lung, kidney, and tumor of the mice bearing 4T1 tumor at 24 h postinjection at the dose of 7.5 mg/kg ICG/DOX, respectively.

of ICG within Vesicles were above 0.2 μg/mL. It indicates that Vesicles are able to disrupt lysosomal membranes under irradiation, possibly resulting from their enhanced photostability, and stronger ability to generate singlet oxygen and subsequent damage on lysosomal membranes even at a low concentration of ICG.[13,27,29] Moreover, it also shows that the lysosomal disruption is independent of photothermal effect since Vesicles could only generate negligible photothermal effect at a very low concentration (*e.g.*, 0.2 μg/mL ICG). The lysosomal disruption can translocate more Vesicles and released DOX into the cytoplasma (Figure 4D), in which released DOX can easily access the nucleus for achieving its enhanced cytotoxicity.[10,13] Obviously, cyanine dye as a multifunctional agent has a remarkable influence on intracellular delivery of anticancer drug under irradiation.

To demonstrate the photothermal cytotoxicity of Vesicles against cancer cells, we first incubated 4T1 cells with the vesicles encapsulating ICG alone (ICG-Vesicles) in the absence of DOX for 24 h, followed by 3 min irradiation at various intensities. ICG-Vesicles without irradiation had negligible cytotoxicity (Figure 5A). However, ICG-Vesicles exhibited a remarkable photothermal cytotoxicity against 4T1 cells under 1.5 W/cm^2 irradiation ($\sim$12.0 μg/mL half growth inhibition concentration, IC_{50}), which was also related with the irradiation intensity. Subsequently, we further demonstrated the synergistic cytotoxicity of Vesicles between photothermal injury from ICG and chemotherapy from DOX against 4T1 cells. Figure 5B shows that Vesicles had the IC_{50} value of 0.2 μg/mL under irradiation, and exhibited significant cytotoxicity advantage over ICG-Vesicles under irradiation (IC_{50}, 12.0 μg/mL), Vesicles without irradiation (IC_{50}, 0.7 μg/mL), and free ICG/DOX under irradiation (IC_{50}, 3.0 μg/mL).[44] It indicates that synergistic thermo-chemotherapy of Vesicles under irradiation is much stronger than the chemotherapy or PTT of Vesicles alone. In contrast, Micelles as the control had the IC_{50} value of 0.5 μg/mL under irradiation, indicating a less cytotoxicity as compared to Vesicles under irradiation. Obviously, the multiple theranostic features of Vesicles synergistically contribute to their superior therapeutic efficiency including stimuli-responsive releases, enhanced photothermal conversion efficiency, higher cellular uptakes, and efficient intracellular translocation of DOX.

Pharmacokinetic Behavior, Biodistribution, and *in Vivo* NIRF Imaging. First, we evaluated the pharmacokinetic behaviors of free ICG/DOX, Micelles, and Vesicles (Supporting Information Figure S14). It indicates that Vesicles exhibited a longer elimination half-life ($t_{1/2\beta}$) of 25.9 h when compared with that of Micelles (16.7 h) and free DOX (3.2 h) (Supporting Information Table S2). The area under the curve ($AUC_{0\sim\infty}$) value of Vesicles was 28 times higher than that of free DOX. Remarkably, Vesicles provide a preferable long-circulation effect as compared to Micelles and free DOX. Next, we evaluated the biodistribution features of Vesicles on the mice bearing

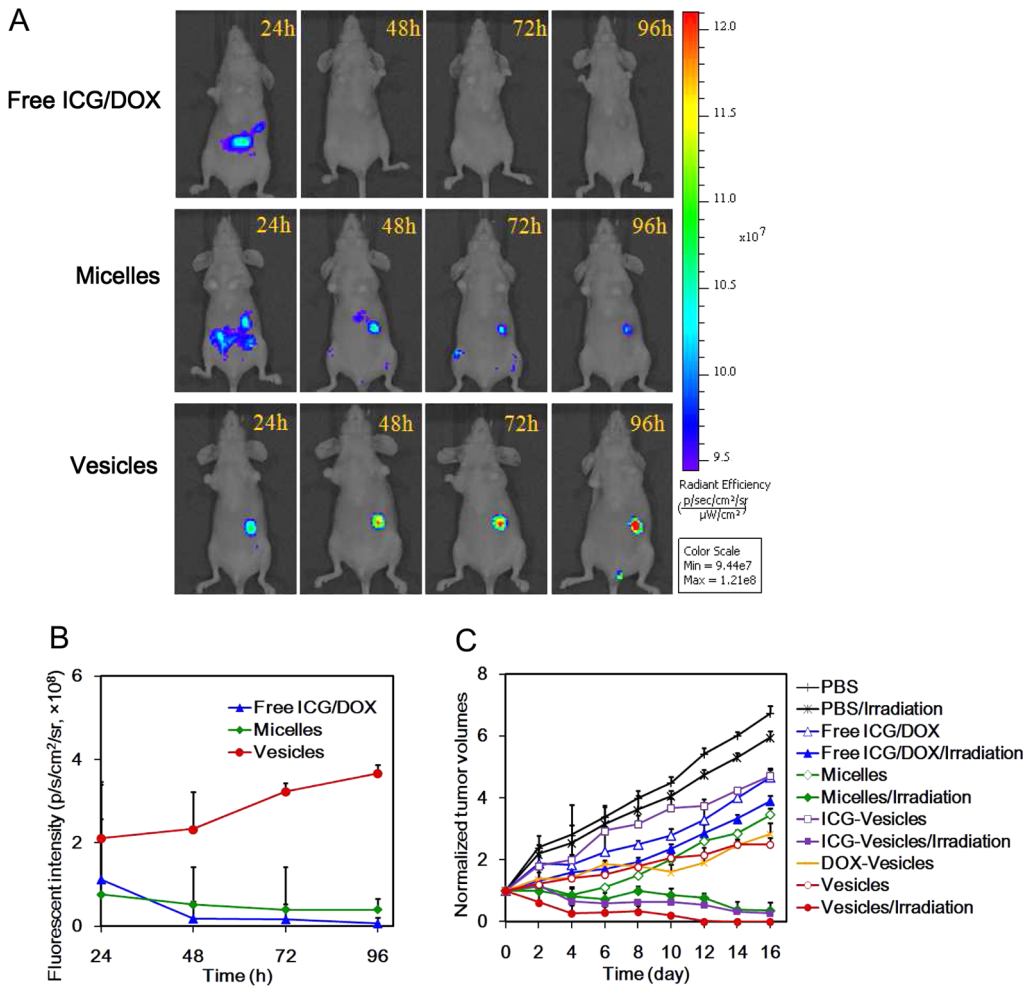

Figure 6. (A) *In vivo* NIRF images and (B) NIRF intensities of the mice bearing 4T1 tumor injected with Vesicles, Micelles and free ICG/DOX at the dose of 7.5 mg/kg ICG/DOX at 24, 48, 72, and 96 h postinjection (n = 3), respectively. (C) Tumor growth inhibition profiles of the mice bearing 4T1 tumor injected with Vesicles, ICG−Vesicles, DOX−Vesicles, Micelles, and free ICG/DOX at the dose of 7.5 mg/kg ICG/DOX under 1.0 W/cm^2 irradiation (785 nm, 5 min) at 24 h postinjection (n = 3), respectively.

4T1 tumors. Both ICG and DOX from Vesicles were mainly distributed into tumors at 24 h postinjection (Figure 5C,D, and Supporting Information Figure S15). Vesicles exhibited 2.6-fold and 3.0-fold increases of the accumulations of ICG and DOX at tumors as compared to free ICG/DOX, respectively, possibly owing to their long-circulation effect, and enhanced permeation and retention (EPR) effect.[45,46] In contrast, Micelles only exhibited 1.6-fold and 2.0-fold increases of ICG and DOX as compared to free ICG/DOX at tumors.[30] Obviously, Vesicles can lead to the enhanced tumor accumulations of ICG and DOX, possibly resulting from their higher surface concentration of PEG and thus longer circulation as compared to those of Micelles, even though Micelles have smaller size.[34,47]

To demonstrate the imaging capacity of Vesicles, we evaluated their *in vivo* NIRF imaging on the mice bearing 4T1 tumors.[28,30] Free ICG/DOX and Micelles had low NIRF signals at tumor and quick elimination of signals at tumors afterward during 4 days (Figure 6A,B). Interestingly, Vesicles exhibited a continuous increase of NIRF signals at tumor during 4 days, followed with low noise at normal tissues. The NIRF signals of Vesicles at 24 and 96 h postinjection were 2.1 × 10^8 and 3.7 × 10^8 p/s/cm^2/sr at tumors, respectively, which had the 2.7-fold and 9.5-fold increases of signals as compared to those of Micelles (Figure 6B). Obviously, Vesicles exhibit ultrahigh imaging contrast during a long-term imaging period, possibly resulting from the enhanced accumulation and retention of ICG at tumors,[45,46] and its quick elimination at normal tissues.[27,30,48] Moreover, the enhanced stability of ICG in Vesicles at pH 5.0 (Supporting Information Figure S10), and fluorescent dequenching from released ICG might also account for the increase of fluorescent signals at tumors (Supporting Information Figure S16).[2,12,15,49] So far, most of cyanine-based probes are reported to exhibit limited imaging contrast owing to their quick elimination at tumors.[26] It is an effective strategy to improve imaging contrast using Vesicles as the vehicle.[12]

***In Vivo* Anticancer Efficacy and Haematoxylin & Eosin (H&E) Staining.** We further demonstrate the *in vivo* synergistic

anticancer efficacy of Vesicles on the mice bearing 4T1 tumors.[30] Vesicles without irradiation exhibited 2.4-fold increase of tumor volumes after 15 days postinjection, which was similar to that of the vesicles encapsulating DOX alone (DOX-Vesicles) (2.8-fold increase) (Figure 6C). Obviously, Vesicles without ICG had the enhanced chemotherapeutic efficacy compared to free ICG/DOX owing to the enhanced biodistribution and cellular uptake of DOX. Importantly, Vesicles caused the necrosis and regression of tumors at 4−6 days postinjection upon irradiation, and resulted in complete tumor ablation after 12 days postinjection (Supporting Information Figure S17). Remarkably, vesicles under irradiation are much more efficient than DOX-Vesicles with alone chemotherapy or ICG-Vesicles with alone PTT. On the other hand, Vesicles also exhibited much stronger tumor inhibition effect than Micelles under irradiation or not, possibly owing to the synergy of enhanced photothermal damage and chemotherapeutic effect triggered by the multiple advantages including enhanced photothermal conversion efficiency, sustained release, higher cellular uptake, efficient intracellular drug translocation, as well as enhanced tumor accumulation.[29,30,32,50] Finally, the H&E staining further indicates that Vesicles resulted in more remarkable cell necrosis and extensive hemorrhagic inflammation under irradiation as compared to free ICG/DOX and Micelles (Supporting Information Figure S18), while normal tissues did not suffer from the damage from PTT and chemotherapy of Vesicles (Supporting Information Figure S19).[27] It validates that Vesicles are able to trigger more severe damages on tumors under synergistic treatment as compared to free ICG/DOX and Micelles, owing to their enhanced tumor accumulation, higher chemotherapeutic efficiency, and stronger hyperthermia, which play a key role for achieving subsequent tumor ablation.

CONCLUSION

We have successfully synthesized pH/reduction-cleavable star terpolymer, which was used to construct nanoscale Vesicles with monodispersive size distribution. Vesicles possess smart on-demand releases of cyanine dye and anticancer drug, and enhanced photothermal conversion efficiency mediated by nonradiative transition of vesicular nanostructures. Vesicles trigger ultrahigh imaging contrast owing to its enhanced tumor accumulation and retention, and subsequent fluorescence dequenching, and simultaneously cause optimal thermo-chemotherapy-synergized tumor ablation mediated by the multiple features including stronger photothermal effect, efficient intracellular drug translocation from lysosomes to cytoplasm, as well as enhanced cellular uptakes and tumor accumulations. Until now, a number of polymeric vesicles consisting of copolymers have been explored as drug carrier, and there are only a few reports about smart vesicles for theranostic application.[22,34,51] Our proof-of-concept design of dually pH/reduction-responsive terpolymeric vesicles represents a versatile approach for both enhanced cancer imaging and synergistic cancer therapy with tumor ablation.

MATERIALS AND METHODS

Preparation of Vesicles. Two milligrams of ICG, 2.0 of mg DOX and 6.0 mg of $PEG_{45}-PCL_{60}-PNIPAM_{33}$ were mixed with 5.0 mL of DMSO, and then the mixed solution was dispersed into 50 mL of distilled water under ultrasonication (5 min). Subsequently, the ICG/DOX-loaded terpolymeric vesicles were obtained after the purification *via* the dialysis (Cut-off 3.5 K MW, 24 h). All the above procedures were performed at 37 °C. The same procedures were used to prepare ICG-loaded $PEG_{45}-PCL_{60}-PNIPAM_{33}$ vesicles without DOX (ICG-Vesicles, 20% loading) or DOX-loaded $PEG_{45}-PCL_{60}-PNIPAM_{33}$ vesicles without ICG (DOX-Vesicles, 20% loading). The same procedures were also performed for preparing the ICG/DOX-loaded PEG_{45}-PCL_{60} Micelles as the control without stimuli-responsiveness. Free ICG/DOX as the mixture of free ICG and DOX was afforded by dissolving ICG and DOX in 5% DMSO.

Characterization. The hydrodynamic diameters of samples were measured using Zetasizer ZS90 (Malvem, U.K.) at 25 °C. The morphology of samples was observed using Transmission electron microscope (TEM, Tecnai-G20). The drug loading and entrapment efficiency of ICG and DOX within Vesicles were evaluated using ultrafiltration centrifuge (Cut-off 10 K MW) at 4 °C. The absorbance and fluorescent spectra of ICG or DOX were measured using UV−vis Spectrophotometer (UV2600, Shimadzu) and Fluorescence Spectrophotometer (LS 55, PerkinElmer), respectively.

Fluorescence Lifetime and Singlet Oxygen Quantum Yield. The solutions of Vesicles, Micelles and free ICG in aqueous solutions at 10.0 μg/mL ICG were prepared. Fluorescence lifetime of each sample measured in triplicate using Fluorescence Lifetime Spectrometer (QM40, Photon Technology International) with a 463 nm excitation source and the detector of 830 nm. The results represent average values ± SD (n = 3). For singlet oxygen quantum yield (Φ_Δ) measurement, different formulations including Free ICG/DOX, Micelles and Vesicles were evaluated using 1,3-disphenylisobenzofuran (DPBF) as a chemical quencher and zinc phthalocyanine (ZnPc) as a reference compound (Φ_Δ^{ZnPc} = 0.67).[52] The solutions of ZnPc (10 μM) and various formulations (20 μM) containing DPBF (30 μM) were irradiated using 660 nm laser at 600 mW/cm^2, and 785 nm laser at 600 mW/cm^2, respectively. Each sample was irradiated for 240 s, and the absorbance of DPBF at 417 nm was measured every 30 s (n = 3). The values of Φ_Δ were calculated using the following relationship $\Phi_\Delta = \Phi_\Delta^{ZnPc} \cdot W \cdot I^{ZnPc} / (W^{ZnPc} \cdot I)$, where W and W^{ZnPc} are the DPBF photobleaching rates in the presence of ICG and ZnPc, respectively. I and I^{ZnPc} are the rates of light absorption by ICG and ZnPc, respectively.

Drug Release. The drug release behaviors of ICG and DOX from various formulations were evaluated using dialysis method. Free ICG/DOX and Micelles were used as the control. The various formulations (each 1.0 mL) were, separately, added in the various solutions including the buffers at pH 5.0 and pH 7.4 in the presence and absence of 10 mM DTT. Then, the *in vitro* releases were performed in air Contrast Temperature Oscillator shaker at 37 °C. Each 1.0 mL sample was taken from the release medium at 0.17, 0.5, 1, 2, 4, 8, 12, 16, 24, and 48 h with the addition of fresh medium. UV−vis spectrometer and Fluorescence Spectrophotometer were used to measure

the concentrations of ICG and DOX, respectively. The results represent average values ± SD (n = 3).

Photothermal Effect. Free ICG/DOX, Micelles and Vesicles (each 0.3 mL) at the concentrations of 1, 2, 5, 10, 25, and 50 μg/mL ICG were, separately, stored in the glass vials and then were irradiated at 785 nm (1.5 W/cm^2). Meanwhile, the temperature of the solution was measured using a thermometer during 300 s. PBS was used as the control in this experiment. The results represent average values ± SD (n = 3).

Photostability. Free ICG/DOX, Micelles and Vesicles (10 μg/mL ICG, each 0.5 mL) were irradiated at 785 nm (1.5 W/cm^2) for 0, 0.5, 1, 2, 3, 5, 7, and 10 min, separately. The absorbance of ICG was measured using a UV−vis Spectrophotometer.

Stability. Free ICG/DOX, Micelles, and Vesicles (each 2.0 mL, 50 μg/mL ICG) were dispersed into serum, cell culture medium, and buffers at pH 7.4 and pH 5.0 (each 8.0 mL) at 25 °C. The absorbance and fluorescent spectra of ICG or DOX were measured after 0, 4, 8, 12, 24, and 48 h.

Cellular Uptakes. 4T1 cells were seeded on 24-well plates (3×10^5 cells/well) and incubated overnight in RPMI 1640 medium containing 10% FBS. Free ICG/DOX, Micelles, and Vesicles (4 μg/mL ICG) were separately added into the wells. After 24 h incubation, the cells were washed 3 times with PBS. The cells were then incubated with 0.5 mL of trypsin (Sigma-Aldrich) for 3 min at 37 °C, and counted after centrifuge collection, followed by ultrasonication. Then, ICG and DOX from the cells were extracted using methanol. Finally, the concentrations of ICG and DOX were measured using UV−vis and fluorescent assay, respectively.

Endocytotic Pathways. 4T1 cells (1×10^6 cells/well) were seeded in 6-well plates for 12 h incubation. Then, PBS as the control and various inhibitors including chlorpromazine (clathrin, 10.0 μg/mL), filipin (caveolae, 5.0 μg/mL), and amiloride (macropinocytosis, 100.0 μg/mL) were used in serum-free RPMI 1640 medium for 1 h at 37 or 4 °C, separately. Then, Vesicles (4.0 μg/mL DOX) were further added for 1 h incubation. Subsequently, the cells were washed 3 times using PBS, treated with trypsin, centrifuged at 4 °C, and finally suspended in 0.5 mL of PBS. The fluorescent intensity of DOX in cells was analyzed using flow cytometry (BD LSR II).

Intracellular Distribution Using CLSM. 4T1 cells (5.0×10^4 cells/well) were seeded in a glass-bottom dish with 1.0 mL of culture medium for 24 h. Then, the cells were incubated with Vesicles for 0.5 h at 37 °C, and further subjected to the presence or absence of 3 min irradiation (785 nm, 1.5 W/cm^2). Afterward, the cells were washed using PBS. Subsequently, 1.0 mL of RPMI 1640 medium containing 200 μL of Lysotraker Green DND-26 (100 nM) was added and the mixture was incubated for another 5 min at 37 °C. Then, Hoechst 33342 was added and the mixture was incubated for another 10 min. Finally, the cells were rinsed with PBS and observed using CLSM (Zeiss LSM710).

Observation of Lysosomal Disruption. AO was employed as an intracellular indicator of acidic lysosomes. AO in lysosomes emits a red fluorescence (yellow after overlap), and generates green fluorescence in nuclei and cytoplasma. When acidic lysosomes are disrupted, the red fluorescence from AO may disappear and only green fluorescence can be observed. In this study, 4T1 cells were seeded overnight on glass slides in 35 mm dishes, and treated with PBS and Vesicles at the doses of 0.2, 0.5, and 2.0 μg/mL ICG for 6 h, respectively. Then, the cells were incubated in fresh medium, followed by 3 min irradiation at 1.5 W/cm^2. After 1 h, the cells were washed using PBS and further incubated with 6.0 μM AO (1.0 mL) for 15 min. The cells were observed using CLSM after wash (Zeiss LSM 710).

MTT Assay. For photothermal cytotoxicity, the cells were incubated with ICG-Vesicles containing various concentrations of ICG including 0.1, 0.5, 4, 12, 24, and 48 μg/mL for 24 h, and then subjected to 3 min irradiation at 1.0, 1.5, and 3.0 W/cm^2. Subsequently, the cell viability was measured using MTT assay. For synergistic cytotoxicity, 4T1 cells were incubated with different formulations including free ICG/DOX, Micelles and Vesicles at various concentrations including 0.05, 0.1, 0.2, 0.5, 1.0, 2.0, and 4.0 μg/mL for 24 h in the presence or absence of 3 min irradiation (785 nm, 1.5 W/cm^2), and then the cells were washed using PBS. After 24 h, the cell viability was evaluated using MTT assay.

Pharmacokinetic Behavior. Female Balb/c mice (18−20 g) were randomly divided into three groups (5 mice per group) and injected intravenously through the tail vein with free ICG/DOX, Micelles or Vesicles (7.5 mg/kg DOX). The blood samples were drawn from the orbits at 0.17, 0.5, 1, 2, 6, 12, and 24 h post-injection, and centrifuged for 10 min at 14 000 rpm at 4 °C for isolating the plasma, followed by the storage at −20 °C. The plasma samples were mixed with methanol and centrifuged for 10 min at 14 000 rpm at 4 °C in order to remove proteins. The concentrations of DOX were determined using a reversed-phased high performance liquid chromatography (Angilent1100) equipped with a reversed-phase column (AlltimaTM C18 5 μm, 4.6 mm × 250 mm) at the wavelength of 227 nm and 25 °C.

Biodistribution. The female BALB/c mice (16−18 g) bearing the tumor-bearing mice were constructed *via* the subcutaneous injection of 4T1 cells (2×10^6 cells/each mouse). Then, the tumor-bearing mice were injected intravenously with free ICG/DOX, Micelles and Vesicles at the doses of 7.5 mg/kg ICG and 7.5 mg/kg DOX. Then, the various tissues including heart, liver, spleen, lung, kidney and tumor were extracted from the mice at 24 h postinjection and finally imaged using IVIS Lumina II (745 nm excitation). The NIRF signals of ICG from free ICG/DOX, Micelles and Vesicles in the various tissues were quantified to demonstrate the *ex vivo* biodistribution of ICG at 24 h postinjection. Afterward, the tissues were further homogenized in 1.0 mL of physiological saline. Then, methanol and chloroform were used to extract DOX from the solutions, and finally, the HPLC analysis was used to measure the biodistribution of DOX.

***In Vivo* Imaging.** Free ICG/DOX, Micelles and Vesicles were injected intravenously into the Balb/c nude mice bearing 4T1 tumors at the dose of 7.5 mg/kg ICG (n = 3). Then, the mice were observed using IVIS Lumina II under 745 nm excitation at 24, 48, 72, and 96 h postinjection. The average NIRF intensity at tumor was quantified at different time.

***In Vivo* Efficacy.** 4T1 cells (2×10^6 cells/each mouse) were subcutaneously transplanted into the flanks of the female Balb/c mice. When the tumors reached a size of 50−80 mm^3 (about 7 days after transplantation), various formulations including PBS, free ICG/DOX (7.5 mg/kg ICG and 7.5 mg/kg DOX), Micelles (7.5 mg/kg ICG and 7.5 mg/kg DOX), DOX-Vesicles (7.5 mg/kg DOX), ICG-Vesicles (7.5 mg/kg ICG) and Vesicles (7.5 mg/kg ICG and 7.5 mg/kg DOX) were injected intravenously into the mice (3 mice/each group) on day 0, 2, and 4. Subsequently, the tumors were irradiated for 5 min (785 nm, 1.0 W/cm^2) or not irradiated at all at 24 h postinjection. The tumor volumes (V) were measured as follows: $V = L \times W^2/2$, where W is the tumor size at the widest point, and L is the tumor size at the longest dimension. The mice were sacrificed by cervical dislocation under an anesthetic status at 16 days postinjection. The results represent average values ± SD (n = 3). The statistic difference was analyzed using t-test where P-value of <0.05 is considered significant.

***Ex Vivo* Histological Staining.** The various formulations including PBS, free ICG/DOX, Micelles and Vesicles were injected intravenously into the Balb/c mice bearing 4T1 tumors (~60 mm^3) at a single dose of 7.5 mg/kg ICG. Then, the tumors suffered from 5 min irradiation (785 nm, 1.0 W/cm^2) at 24 h postinjection. The tumor, heart, liver, spleen, lung, and kidney were dissected from the mice at 6 h postirradiation, and fixed in a 4% formaldehyde solution for 24 h at room temperature. The various tissues were frozen, and the sections with the thickness of 10 μm were made on a cryostat. The H&E staining (BBC Biochemical, Mount Vernon, WA) was performed, and further observed using an IX73 bright field microscopy (Olympus).

Conflict of Interest: The authors declare no competing financial interest.

Supporting Information Available: Synthetic route, ^{1}H NMR spectra, IR spectra, GPC analysis, release profiles, chemical stability, AO staining, *ex vivo* imaging, fluorescent dequenching, photo of tumors, and H&E staining. The Supporting Information is available free of charge on the ACS Publications website at DOI: 10.1021/acsnano.5b02843.

Acknowledgment. We thank National Natural Science Foundation of China (31422021, 51473109, 81202472, 21074081 and 21274096), National Basic Research Program of China

(2012CB932500 and 2014CB931903), the Priority Academic Program Development (PAPD) of Jiangsu Higher Education Institutions, and Jiangsu Key Laboratory of Translational Research and Therapy for Neuro-Psycho-Diseases (BM2013003).

REFERENCES AND NOTES

1. Cabral, H.; Nishiyama, N.; Kataoka, K. Supramolecular Nanodevices: from Design Validation to Theranostic Nanomedicine. *Acc. Chem. Res.* **2011**, *44*, 999–1008.
2. Melancon, M. P.; Zhou, M.; Li, C. Cancer Theranostics with Near-Infrared Light-Activatable Multimodal Nanoparticles. *Acc. Chem. Res.* **2011**, *44*, 947–956.
3. Wang, A. Z.; Langer, R.; Farokhzad, O. C. Nanoparticle Delivery of Cancer Drugs. *Annu. Rev. Med.* **2012**, *63*, 185–198.
4. Jain, R. K.; Stylianopoulos, T. Delivering Nanomedicine to Solid Tumors. *Nat. Rev. Clin. Oncol.* **2010**, *7*, 653–664.
5. Gindy, M. E.; Prud'homme, R. K. Multifunctional Nanoparticles for Imaging, Delivery and Targeting in Cancer Therapy. *Expert Opin. Drug Delivery* **2009**, *6*, 865–878.
6. Chapman, S.; Dobrovolskaia, M.; Farahani, K.; Goodwin, A.; Joshi, A.; Lee, H.; Meade, T.; Pomper, M.; Ptak, K.; Rao, J.; et al. Nanoparticles for Cancer Imaging: the Good, the Bad, and the Promise. *Nano Today* **2013**, *8*, 454–460.
7. Kamaly, N.; Xiao, Z.; Valencia, P. M.; Radovic-Moreno, A. F.; Farokhzad, O. C. Targeted Polymeric Therapeutic Nanoparticles: Design, Development and Clinical Translation. *Chem. Soc. Rev.* **2012**, *41*, 2971–3010.
8. Peer, D.; Karp, J. M.; Hong, S.; Farokhzad, O. C.; Margalit, R.; Langer, R. Nanocarriers as an Emerging Platform for Cancer Therapy. *Nat. Nanotechnol.* **2007**, *2*, 751–760.
9. Ge, Z.; Liu, S. Functional Block Copolymer Assemblies Responsive to Tumor and Intracellular Microenvironments for Site-Specific Drug Delivery and Enhanced Imaging Performance. *Chem. Soc. Rev.* **2013**, *42*, 7289–7325.
10. Nomoto, T.; Fukushima, S.; Kumagai, M.; Machitani, K.; Arnida; Matsumoto, Y.; Oba, M.; Miyata, K.; Osada, K.; Nishiyama, N.; et al. Three-Layered Polyplex Micelle as a Multifunctional Nanocarrier Platform for Light-Induced Systemic Gene Transfer. *Nat. Commun.* **2014**, *5*, 3545.
11. Mura, S.; Nicolas, J.; Couvreur, P. Stimuli-Responsive Nanocarriers for Drug Delivery. *Nat. Mater.* **2013**, *12*, 991–1003.
12. Wang, Y.; Zhou, K.; Huang, G.; Hensley, C.; Huang, X.; Ma, X.; Zhao, T.; Sumer, B. D.; DeBerardinis, R. J.; Gao, J. A Nanoparticle-Based Strategy for the Imaging of a Broad Range of Tumours by Nonlinear Amplification of Microenvironment Signals. *Nat. Mater.* **2014**, *13*, 204–212.
13. Nishiyama, N.; Iriyama, A.; Jang, W. D.; Miyata, K.; Itaka, K.; Inoue, Y.; Takahashi, H.; Yanagi, Y.; Tamaki, Y.; Koyama, H.; et al. Light-Induced Gene Transfer from Packaged DNA Enveloped in a Dendrimeric Photosensitizer. *Nat. Mater.* **2005**, *4*, 934–941.
14. Cabral, H.; Matsumoto, Y.; Mizuno, K.; Chen, Q.; Murakami, M.; Kimura, M.; Terada, Y.; Kano, M. R.; Miyazono, K.; Uesaka, M.; et al. Accumulation of Sub-100 nm Polymeric Micelles in Poorly Permeable Tumours Depends on Size. *Nat. Nanotechnol.* **2011**, *6*, 815–823.
15. Lovell, J. F.; Liu, T. W.; Chen, J.; Zheng, G. Activatable Photosensitizers for Imaging and Therapy. *Chem. Rev.* **2010**, *110*, 2839–2857.
16. Ganta, S.; Devalapally, H.; Shahiwala, A.; Amiji, M. A Review of Stimuli-Responsive Nanocarriers for Drug and Gene Delivery. *J. Controlled Release* **2008**, *126*, 187–204.
17. Du, J. Z.; Du, X. J.; Mao, C. Q.; Wang, J. Tailor-Made Dual pH-Sensitive Polymer-Doxorubicin Nanoparticles for Efficient Anticancer Drug Delivery. *J. Am. Chem. Soc.* **2011**, *133*, 17560–17563.
18. Zhou, K.; Liu, H.; Zhang, S.; Huang, X.; Wang, Y.; Huang, G.; Sumer, B. D.; Gao, J. Multicolored pH-Tunable and Activatable Fluorescence Nanoplatform Responsive to Physiologic pH Stimuli. *J. Am. Chem. Soc.* **2012**, *134*, 7803–7811.
19. Palma, A.; Alvarez, L. A.; Scholz, D.; Frimannsson, D. O.; Grossi, M.; Quinn, S. J.; O'Shea, D. F. Cellular Uptake Mediated off/on Responsive Near-Infrared Fluorescent Nanoparticles. *J. Am. Chem. Soc.* **2011**, *133*, 19618–19621.
20. Zhou, K.; Wang, Y.; Huang, X.; Luby-Phelps, K.; Sumer, B. D.; Gao, J. Tunable, Ultrasensitive pH-Responsive Nanoparticles Targeting Specific Endocytic Organelles in Living Cells. *Angew. Chem., Int. Ed.* **2011**, *50*, 6109–6114.
21. Murakami, M.; Cabral, H.; Matsumoto, Y.; Wu, S.; Kano, M. R.; Yamori, T.; Nishiyama, N.; Kataoka, K. Improving Drug Potency and Efficacy by Nanocarrier-Mediated Subcellular Targeting. *Sci. Transl. Med.* **2011**, *3*, 64ra2.
22. Lovell, J. F.; Jin, C. S.; Huynh, E.; Jin, H.; Kim, C.; Rubinstein, J. L.; Chan, W. C.; Cao, W.; Wang, L. V.; Zheng, G. Porphysome Nanovesicles Generated by Porphyrin Bilayers for Use as Multimodal Biophotonic Contrast Agents. *Nat. Mater.* **2011**, *10*, 324–332.
23. Gao, G. H.; Lee, J. W.; Nguyen, M. K.; Im, G. H.; Yang, J.; Heo, H.; Jeon, P.; Park, T. G.; Lee, J. H.; Lee, D. S. pH-Responsive Polymeric Micelle Based on PEG-Poly(Beta-Amino Ester)/(Amido Amine) as Intelligent Vehicle for Magnetic Resonance Imaging in Detection of Cerebral Ischemic Area. *J. Controlled Release* **2011**, *155*, 11–17.
24. Hirsjarvi, S.; Passirani, C.; Benoit, J. P. Passive and Active Tumour Targeting with Nanocarriers. *Curr. Drug Discovery Technol.* **2011**, *8*, 188–196.
25. Luo, S.; Zhang, E.; Su, Y.; Cheng, T.; Shi, C. A Review of NIR Dyes in Cancer Targeting and Imaging. *Biomaterials* **2011**, *32*, 7127–7138.
26. Escobedo, J. O.; Rusin, O.; Lim, S.; Strongin, R. M. NIR Dyes for Bioimaging Applications. *Curr. Opin. Chem. Biol.* **2010**, *14*, 64–70.
27. Guo, M.; Mao, H.; Li, Y.; Zhu, A.; He, H.; Yang, H.; Wang, Y.; Tian, X.; Ge, C.; Peng, Q.; et al. Dual Imaging-Guided Photothermal/Photodynamic Therapy using Micelles. *Biomaterials* **2014**, *35*, 4656–4666.
28. Yang, H.; Mao, H.; Wan, Z.; Zhu, A.; Guo, M.; Li, Y.; Li, X.; Wan, J.; Yang, X.; Shuai, X.; et al. Micelles Assembled with Carbocyanine Dyes for Theranostic Near-Infrared Fluorescent Cancer Imaging and Photothermal Therapy. *Biomaterials* **2013**, *34*, 9124–9133.
29. Chen, H.; Xiao, L.; Anraku, Y.; Mi, P.; Liu, X.; Cabral, H.; Inoue, A.; Nomoto, T.; Kishimura, A.; Nishiyama, N.; Kataoka, K. Polyion Complex Vesicles for Photoinduced Intracellular Delivery of Amphiphilic Photosensitizer. *J. Am. Chem. Soc.* **2014**, *136*, 157–163.
30. Wan, Z.; Mao, H.; Guo, M.; Li, Y.; Zhu, A.; Yang, H.; He, H.; Shen, J.; Zhou, L.; Jiang, Z.; et al. Highly Efficient Hierarchical Micelles Integrating Photothermal Therapy and Singlet Oxygen-Synergized Chemotherapy for Cancer Eradication. *Theranostics* **2014**, *4*, 399–411.
31. Huang, P.; Lin, J.; Wang, X.; Wang, Z.; Zhang, C.; He, M.; Wang, K.; Chen, F.; Li, Z.; Shen, G.; et al. Light-Triggered Theranostics Based on Photosensitizer-Conjugated Carbon Dots for Simultaneous Enhanced-Fluorescence Imaging and Photodynamic Therapy. *Adv. Mater.* **2012**, *24*, 5104–5110.
32. Zhang, Z.; Wang, J.; Nie, X.; Wen, T.; Ji, Y.; Wu, X.; Zhao, Y.; Chen, C. Near Infrared Laser-Induced Targeted Cancer Therapy using Thermoresponsive Polymer Encapsulated Gold Nanorods. *J. Am. Chem. Soc.* **2014**, *136*, 7317–7326.
33. Zheng, M.; Yue, C.; Ma, Y.; Gong, P.; Zhao, P.; Zheng, C.; Sheng, Z.; Zhang, P.; Wang, Z.; Cai, L. Single-Step Assembly of DOX/ICG Loaded Lipid–Polymer Nanoparticles for Highly Effective Chemo-Photothermal Combination Therapy. *ACS Nano* **2013**, *7*, 2056–2067.
34. Lee, J. S.; Feijen, J. Polymersomes for Drug Delivery: Design, Formation and Characterization. *J. Controlled Release* **2012**, *161*, 473–483.
35. Levine, D. H.; Ghoroghchian, P. P.; Freudenberg, J.; Zhang, G.; Therien, M. J.; Greene, M. I.; Hammer, D. A.; Murali, R. Polymersomes: A New Multi-Functional Tool for Cancer Diagnosis and Therapy. *Methods* **2008**, *46*, 25–32.
36. Christian, D. A.; Cai, S.; Bowen, D. M.; Kim, Y.; Pajerowski, J. D.; Discher, D. E. Polymersome Carriers: from Self-Assembly to SiRNA and Protein Therapeutics. *Eur. J. Pharm. Biopharm.* **2009**, *71*, 463–474.
37. Onaca, O.; Enea, R.; Hughes, D. W.; Meier, W. Stimuli-Responsive Polymersomes as Nanocarriers for Drug and Gene Delivery. *Macromol. Biosci.* **2009**, *9*, 129–139.

38. Boyer, C.; Bulmus, V.; Davis, T. P.; Ladmiral, V.; Liu, J.; Perrier, S. Bioapplications of RAFT Polymerization. *Chem. Rev.* **2009**, *109*, 5402–5436.
39. Chiefari, J.; Chong, Y. K.; Ercole, F.; Krstina, J.; Jeffery, J.; Le, T. P. T.; Mayadunne, R. T. A.; Meijs, G. F.; Moad, C. L.; Moad, G.; et al. Living Free-Radical Polymerization by Reversible Addition-Fragmentation Chain Transfer: the RAFT Process. *Macromolecules* **1998**, *31*, 5559–5562.
40. Kolb, H. C.; Finn, M. G.; Sharpless, K. B. Click Chemistry: Diverse Chemical Function from a Few Good Reactions. *Angew. Chem., Int. Ed.* **2001**, *40*, 2004–2021.
41. Dai, J.; Lin, S.; Cheng, D.; Zou, S.; Shuai, X. Interlayer-Crosslinked Micelle with Partially Hydrated Core Showing Reduction and pH Dual Sensitivity for Pinpointed Intracellular Drug Release. *Angew. Chem., Int. Ed.* **2011**, *50*, 9404–9408.
42. Kirchherr, A. K.; Briel, A.; Mader, K. Stabilization of Indocyanine Green by Encapsulation within Micellar Systems. *Mol. Pharmaceutics* **2009**, *6*, 480–491.
43. Lim, D. K.; Barhoumi, A.; Wylie, R. G.; Reznor, G.; Langer, R. S.; Kohane, D. S. Enhanced Photothermal Effect of Plasmonic Nanoparticles Coated with Reduced Graphene Oxide. *Nano Lett.* **2013**, *13*, 4075–4079.
44. Chu, K. F.; Dupuy, D. E. Thermal Ablation of Tumours: Biological Mechanisms and Advances in Therapy. *Nat. Rev. Cancer* **2014**, *14*, 199–208.
45. Anraku, Y.; Kishimura, A.; Kobayashi, A.; Oba, M.; Kataoka, K. Size-Controlled Long-Circulating PICsome as a Ruler to Measure Critical Cut-Off Disposition Size into Normal and Tumor Tissues. *Chem. Commun.* **2011**, *47*, 6054–6056.
46. Anraku, Y.; Kishimura, A.; Oba, M.; Yamasaki, Y.; Kataoka, K. Spontaneous Formation of Nanosized Unilamellar Polyion Complex Vesicles with Tunable Size and Properties. *J. Am. Chem. Soc.* **2010**, *132*, 1631–1636.
47. Photos, P. J.; Bacakova, L.; Discher, B.; Bates, F. S.; Discher, D. E. Polymer Vesicles in vivo: Correlations with PEG Molecular Weight. *J. Controlled Release* **2003**, *90*, 323–334.
48. Miki, K.; Kimura, A.; Oride, K.; Kuramochi, Y.; Matsuoka, H.; Harada, H.; Hiraoka, M.; Ohe, K. High-Contrast Fluorescence Imaging of Tumors in vivo using Nanoparticles of Amphiphilic Brush-Like Copolymers Produced by ROMP. *Angew. Chem., Int. Ed.* **2011**, *50*, 6567–6570.
49. Urano, Y.; Asanuma, D.; Hama, Y.; Koyama, Y.; Barrett, T.; Kamiya, M.; Nagano, T.; Watanabe, T.; Hasegawa, A.; Choyke, P. L.; et al. Selective Molecular Imaging of Viable Cancer Cells with pH-Activatable Fluorescence Probes. *Nat. Med.* **2009**, *15*, 104–109.
50. Fang, R. H.; Zhang, L. Combinatorial Nanotherapeutics: Rewiring, Then Killing, Cancer Cells. *Sci. Signaling* **2014**, *7*, pe13.
51. Sanson, C.; Diou, O.; Thevenot, J.; Ibarboure, E.; Soum, A.; Brulet, A.; Miraux, S.; Thiaudiere, E.; Tan, S.; Brisson, A.; et al. Doxorubicin Loaded Magnetic Polymersomes: Theranostic Nanocarriers for MR Imaging and Magneto-Chemotherapy. *ACS Nano* **2011**, *5*, 1122–1140.
52. Cardillo, J. A.; Jorge, R.; Costa, R. A.; Nunes, S. M.; Lavinsky, D.; Kuppermann, B. D.; Tedesco, A. C.; Farah, M. E. Experimental Selective Choriocapillaris Photothrombosis using a Modified Indocyanine Green Formulation. *Br. J. Ophthalmol.* **2008**, *92*, 276–280.